Mechanical Systems and Signal Processing 23 (2009) 2658–2670

Contents lists available at ScienceDirect

Mechanical Systems and Signal Processing

journal homepage: www.elsevier.com/locate/jnlabr/ymssp

Induction machine condition monitoring using notch-filtered motor current

Serkan Günal [a], Doğan Gökhan Ece [b,*], Ömer Nezih Gerek [b]

[a] Anadolu University, Department of Computer Engineering, Eskisehir, Turkey
[b] Anadolu University, Department of Electric and Electronics Engineering, Eskisehir, Turkey

ARTICLE INFO

Article history:
Received 28 November 2008
Received in revised form
18 March 2009
Accepted 19 May 2009
Available online 2 June 2009

Keywords:
Induction machine
Condition monitoring
Notch-filter
Skewness
Kurtosis

ABSTRACT

This paper presents a new approach to induction motor condition monitoring using notch-filtered motor current signature analysis (NFMCSA). Unlike most of the previous work utilizing motor current signature analysis (MCSA) using spectral methods to extract required features for detecting motor fault conditions, here NFMCSA is performed in time-domain to extract features of energy, sample extrema, and third and fourth cumulants evaluated from data within sliding time window. Six identical three-phase induction motors were used for the experimental verification of the proposed method. One healthy machine was used as a reference, while other five with different synthetic faults were used for condition detection and classification. Extracted features obtained from NFMCSA of all motors were employed in three different and popular classifiers. The proposed motor current analysis and the performance of the features used for fault detection and classification are examined at various motor load levels and it is shown that a successful induction motor condition monitoring system is developed. Developed system is also able to indicate the load level and the type of a fault in multi-dimensional feature space representation. In order to test the generality and applicability of the developed method to other induction motors, data acquired from another healthy induction motor with different number of poles and rated power is also incorporated into the system. In spite of the above difference, the proposed feature set successfully locates the healthy motor within the classification cluster of "healthy motors" on the feature space.

1. Introduction

The simplicity and ruggedness of the squirrel-cage construction are outstanding advantages of an induction motor and make it by far the most commonly used type of motor in sizes ranging from fractional horsepower to grades of industrial applications. Incipient type of mechanical faults such as cracked or broken rotor bars or end-ring, minor bearing damage, and misalignments which do not completely block the rotor, may cause noise and excessive currents and heat during the steady-state operation of the motor [1]. In addition, magnitude of these currents may be lower than the pick up settings of over current relays and consequently the motor may operate until the complete failure resulting the interruption of an industrial process, causing a down time and even effecting other related machinery. Therefore, mechanical faults must be detected at their inception by means of preventive maintenance in order to avoid undesirable motor failures. Considerable

* Corresponding author.
E-mail address: dgece@anadolu.edu.tr (D. Gökhan Ece).

0888-3270/$ - see front matter © 2009 Elsevier Ltd. All rights reserved.
doi:10.1016/j.ymssp.2009.05.011

amount of research have been conducted on condition monitoring and detection of induction motor faults and the surveys in [2,3] cite most of the work in this area. Both invasive and noninvasive methods are used to measure motor vibration, temperature, speed and torque variations for detection of motor abnormalities. However, the most celebrated and often used method of condition monitoring is the motor current signature analysis (MCSA) since the motor current contains required information for fault detection. Well known signal processing tools of Fourier, Wavelet, and Hilbert–Huang transformations are applied to acquired motor current data to extract necessary features for motor fault detection [4–11]. During steady-state operation, induction motors draw noisy and harmonically rich line current due to their nonlinear characteristics. Spectral methods used for MCSA are employed to extract signature identifiers, namely features to be used for fault classification.

One of the most commonly encountered motor failure is the broken rotor bars. This type of fault is known to cause a rise in magnitude at side band frequency components defined by $f_{BR} = (1 \pm 2ks)f_e$. Here, $k = 1, 2, 3, \ldots, f_e$ is the supply frequency, and s is the slip given by $s = (n_s - n)/n_s$ where n_s is the synchronous speed and n is the rotor speed. For $k = 1$ for example, elevated side bands of the supply frequency above a threshold would indicate broken rotor bars. Similar equations for frequencies corresponding to other types of abnormalities such as misalignment and bearing damage are derived in terms of speed and design parameters of an induction motor in the literature. This way, since the frequencies related to different types of faults are known, detection and classification are performed by comparing the corresponding, for example, wavelet transform decomposition coefficients with a threshold [12]. However, monitoring the increase in magnitude at predicted frequencies alone may yield classification errors due to the fact that, in some cases, different faults may give rise to same frequencies. Consequently, an effective detection and classification method should be able to discriminate motor faults from a healthy motor while distinguishing different fault types.

Frequency of induced voltage and resulting current in the rotor circuitry are proportional to slip s and are slightly less than the stator (supply) frequency. Hence, side band frequency components around the fundamental will appear in the frequency spectrum of the motor current drawn from the supply even in steady-state condition. Magnitude and the frequency of these side bands depend upon the load on the motor and vary with the dynamic change in the load. Therefore, it is very difficult to set a certain threshold level to detect broken or cracked rotor bars at varying load conditions. In addition, extracting the magnitude and frequency information of side band components requires analog/digital conversion with very high sampling rate and signal to noise ratio. When the load on the motor is a light one (half of the rated or less) slip is very small and side bands move towards the strong fundamental component and get overshadowed by it. As a result, side bands may not be visible and their spectral information may not be extracted due to the dominant fundamental component.

Bearing defect is another mostly encountered induction motor mechanical fault faced by the industry due to the contamination, corrosion, and improper lubrication. In the case of a bearing defect, abnormal mechanical noise, excessive heating, and some amount of over current due to the slight blocking effect of the defective bearing to the rotating motor shaft will occur. Measuring the motor current alone as a fault diagnostic parameter naturally excludes the information due to the noise, therefore vibration, and heating. Motor would draw some amount of over current (less current to be picked up by protective circuitry) will occur, and, depending on the type of the bearing fault (inner race, outer race, and defective rolling elements), magnitudes of certain frequency components of the motor current would increase. The effects of different bearing faults to the frequency spectrum of the motor current is investigated in the literature [7]. However, without interrupting the running process of an induction motor and disassembling the motor and the bearing, one could not know what type of a bearing fault has occurred and which frequency component should be inspected and compared with a certain threshold.

This work is motivated from the fact that spectral components of motor current other than the fundamental component carry required information for fault detection therefore removing the 50 (or 60) Hz fundamental by means of notch-filtering would not effect the fault detection process [13]. On the contrary, the confusion of a pronounced fundamental is eliminated this way. Another important development towards fault detection in this paper is the utilization of the energy, maxima, skewness, and kurtosis of notch-filtered current waveform within a sliding time window as signature identifiers. This way, the necessity of proper threshold settings at different frequencies for detecting different fault conditions is rendered obsolete. It can be noted that skewness and kurtosis are higher order statistical parameters related to the higher order spectra, which was previously utilized for machine condition diagnosis [15,16,10]. However, the utilization of higher order spectra in [15,16,10] requires the complete bi- and tri-spectra magnitude, whereas our approach utilizes simple parameters derived from the higher order spectra, and their calculation is significantly simple.

The classification of faulty motors with the proposed parameters is performed using three well known classifiers, namely Bayesian, Gaussian mixture model (GMM), and Fisher's linear discriminant analysis (LDA) to verify the effectiveness and the success of the proposed feature set.

In most of the previous works summarized with great number of bibliographical information in [2,3], considered type of faults were mainly either broken rotor bars or defected bearings and developed fault detection and classification methods have been tested using exactly the same motors with one of them always being the healthy reference. However, in this work for developing and testing the proposed algorithm, in addition to the six exactly the same motor with five of them having different fault conditions, a second healthy induction motor with completely different name plate is incorporated into the test set. The second (and completely different) induction motor verified the fact that the selected feature set is capable of providing a robust fault detection system. When the classification algorithm is performed with two healthy

motors and five faulty ones, healthy motors are successfully classified from faulty motors in spite of the clear differences between the healthy motors. Furthermore, the developed method is able to discriminate the load conditions of the motors and physical differences of the same fault type (i.e., different number of broken rotor bars) in three-dimensional feature space representation. Detailed experimental work has been conducted and the results are explained in following sections.

2. Motor current data acquisition

For the experimental verification of the proposed method, six identical induction motors with one healthy reference motor and five with synthetic faults were used in our experiments. All motors are rated as three-phase, 2.2 kW, four-poles, 50 Hz, and 380V_{LL}. Tests were conducted at various loading conditions of 5.0, 4.7, and 4.1 A corresponding 5% overload, full-load, and approximately half-load, respectively. Load test is accomplished by coupling induction motors with a single-phase permanent magnet synchronous generator connected to an adjustable resistive load bank. The fault types and legends describing them all through this work are:

(1) *Class* 1: Healthy motor (healthy),
(2) *Class* 2: Motor with bearing fault type 1 (rb1),
(3) *Class* 3: Motor with bearing fault type 2 (rb2),
(4) *Class* 4: Motor with three broken rotor bars (rot3),
(5) *Class* 5: Motor with five broken rotor bars (rot5),
(6) *Class* 6: Motor with arbitrarily shorted stator winding (sw).

Illustrations of faulty motors and bearings are depicted in Figs. 1–3. Broken rotor bars are realized by punching holes to the rotor bars with a drill. Faulty bearings are disassembled from induction motors that are taken out of service due to the noise and excessive heat, and are obtained from a real industrial induction motor maintenance workshop. Shorted stator winding fault is generated by stripping the insulation of two adjacent coils for a couple of milimeters and soldering them.

Fig. 1. Defective bearings.

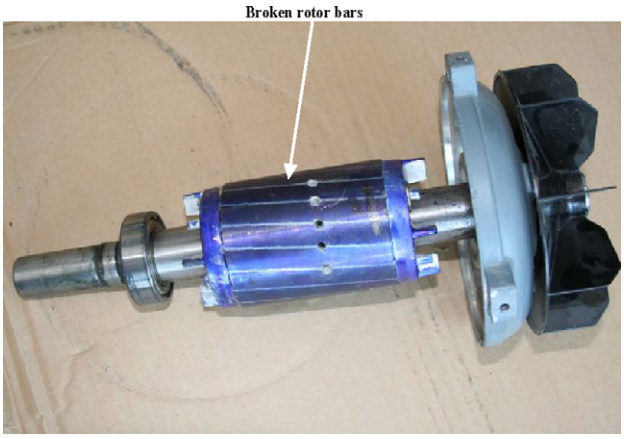

Fig. 2. Broken rotor bars.

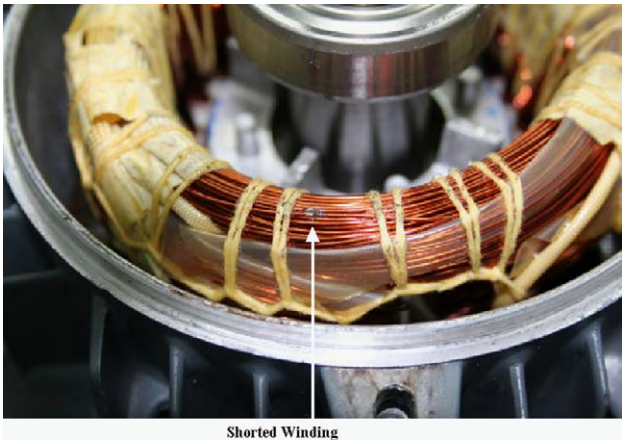

Fig. 3. Shorted stator winding.

Motor current waveform data is acquired from both healthy and faulty motors at a sampling rate of 20 kHz with 16 bit vertical resolution. Real-time notch-filtering is performed with a DSP based programmable filter that is adjusted to 20th order elliptic band-reject filter. A careful inspection of the current waveform reveals that the waveform consists of a fundamental harmonic which constitutes the largest factor of the signal, and a noise-like additive waveform which is relatively subtle and therefore occluded by the fundamental. By eliminating the fundamental harmonic, the subtle details which actually carry the necessary information are emphasized. A properly selected shunt resistance is used as a current sensor. The 40 s-long data is acquired from all six motors for each load condition mentioned above. For the notch-filtered motor current signature analysis (NFMCSA) and feature extraction, acquired data is divided to 0.25 s-long time windows (5000 samples) within which the notched signal may be considered stationary. This way, for each motor considered in this study, we have obtained 160 data sets and the feature vectors consisting of window energy, maxima, skewness, and kurtosis are calculated for each 5000 sample-long time window.

Motor current data and the feature vectors from the second healthy motor with completely different name plate information of three-phase, 1.1 kW, 380 V, 50 Hz are obtained using exactly the same approach used for above mentioned six motors. However, motor-generator set used for the experiments is designed for the 2.2 kW motors and it was not possible to couple the second healthy 1.1 kW motor to the same test bed. Therefore, the motor current data and the feature vectors are obtained from the second healthy motor under no-load condition only. Additionally, the test bed is not equipped to enable experimenting with time-varying loads. Therefore, all conducted experiments were performed under continuous loading. Consequently, the effect of load torque variations to detection and classification of induction motor faults was not observed. Nevertheless, the proposed method should be considered as a tool for preventive maintenance under cooperative conditions of steady load.

3. Feature extraction

Time-domain waveforms for healthy and faulty motor currents acquired at sampling rate of 20 kHz without filtering are illustrated in Fig. 4. Notch-filtered versions of these currents are depicted in Fig. 5. At first visual inspection reveals that original motor currents are quite similar and may not be discriminated easily. The similarity is due to the pronounced fundamental. Consequently, these waveforms may not be directly employed in detection and classification of motor faults due to the presence of the strong fundamental component. On the other hand, notch-filtered current waveforms without the above shadowing effect of the fundamental show visible and unique characteristics for each of the different motor faults. Therefore, one can assume that using the filtered waveforms for the diagnosis of motor faults would yield successful results. This is, in fact, tested as a side experiment, and the same analysis applied to the raw form of current yielded results that are inferior to the results from notch-filtered waveforms. The signature identifiers extracted from the notch-filtered waveforms are energy, maxima, skewness, and kurtosis of sample frames with length of 5000 samples. This way from each acquired motor current data waveform, 160 feature vectors were obtained.

These feature identifiers can be mathematically explained as follows. The frame energy is computed as

$$F1 = \sum_{i=1}^{N} x_i^2, \tag{1}$$

where x_i is the ith sample, and N is the number of samples within the frame. The second feature is the absolute frame maxima, and it is obtained as

$$F2 = \max\{|x_i|, 1 \le i \le N\}. \tag{2}$$

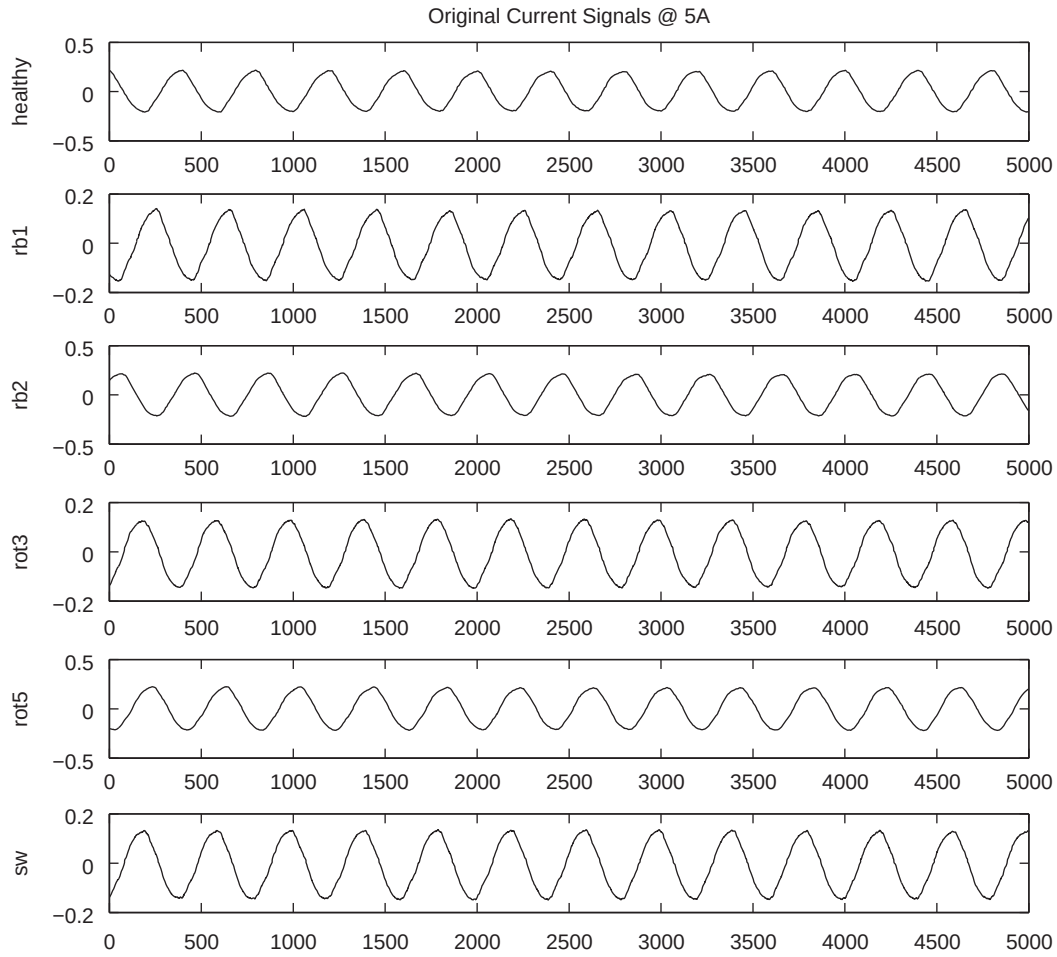

Fig. 4. Original motor currents at 5 A.

The third and the fourth features are kurtosis and skewness calculated for each frame

$$F3 = \frac{\sum_{i=1}^{N}(x_i - m_x)^4}{(N-1)\sigma_x^4} - 3, \tag{3}$$

$$F4 = \frac{\sum_{i=1}^{N}(x_i - m_x)^3}{(N-1)\sigma_x^3}, \tag{4}$$

where m_x corresponds to the sample mean and σ_x corresponds to the sample standard deviation. All these features constitute a four-dimensional feature vector representing the frame. Motor fault analysis is then carried out using these feature vectors extracted from notch-filtered motor current data within a time window.

4. Fault classification and experimental results

As mentioned in Section 2, motor current waveforms were acquired at 20 kHz sampling rate with a duration of 40 s. Therefore, window length of 5000 samples for extracting signature identifiers results in 160 four-dimensional feature vectors for each motor at and each of the selected load levels in this work. Fault detection and classification are performed using three different well known classifiers namely Bayes, GMM, and LDA in order to compare and decide which one of the classifier performs better with selected features.

The first classifier, known as the Bayes classifier works according to a decision rule [14] which minimizes the probability of classification error. A feature vector x is assigned to class c_i among the classes $\{c_1, c_2, \ldots, c_N\}$ if the a-posteriori error statement given below is satisfied:

$$p(x|c_i)p(c_i) > p(x|c_j)p(c_j), \quad j = 1, \ldots, N, \ j \neq i. \tag{5}$$

Usually, a Gaussian distribution is assumed for the probability density functions.

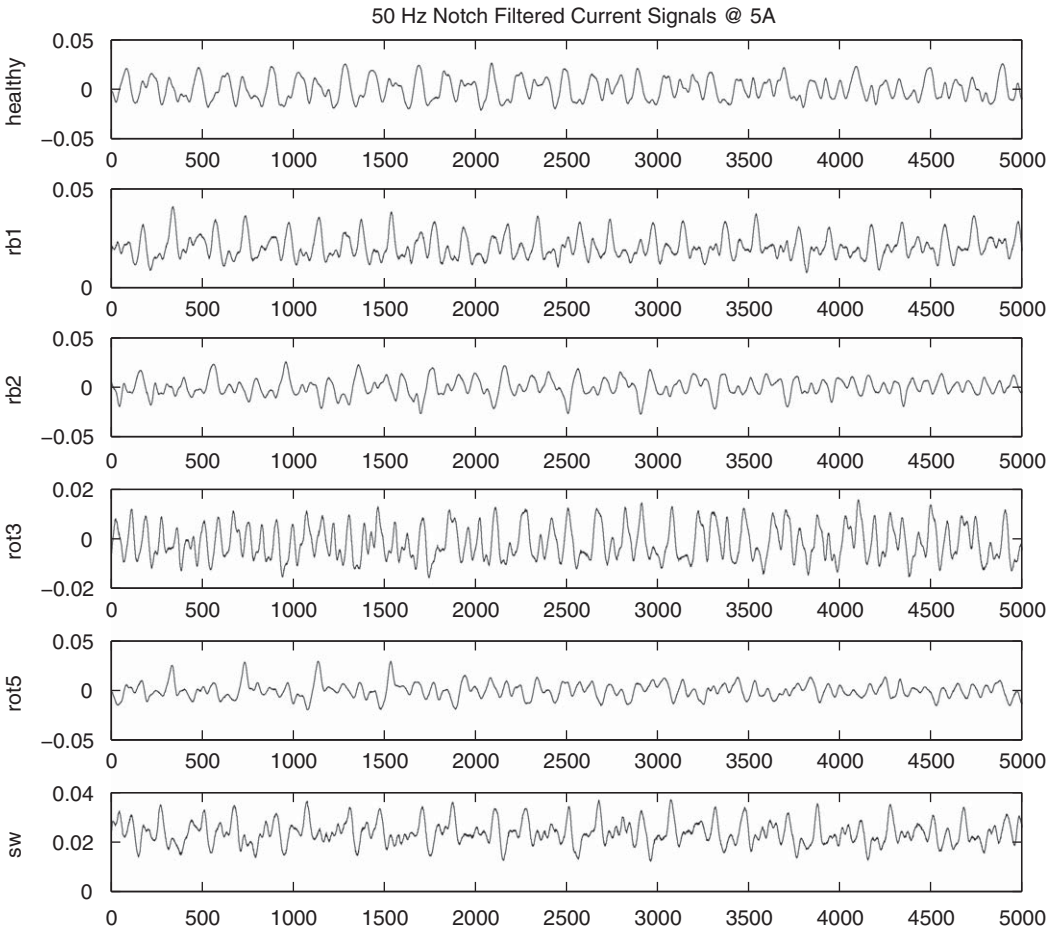

Fig. 5. Notch-filtered motor currents at 5 A.

The second classifier utilizes a variation of the Bayes method with Gaussian mixture models. Gaussian Mixture Model is the combination of multiple (two or more) Gaussian distributions. After application of the model, the same Bayes probability maximization procedure is carried out.

The last classifier depends on Fisher's linear discriminant analysis, which was developed in [17]. This classifier utilizes both within- and between-class scatters where features are projected onto a subspace which minimizes the distance between members of the same class while maximizing the distance to members of the remaining classes. To find a transformation for the regarding subspace, the following criterion function is maximized:

$$J(W) = \frac{|W^T S_B W|}{|W^T S_W W|}, \tag{6}$$

where W is the transformation matrix, and S_B and S_W denote the between-class and within-class scatter, respectively. Solution of this maximization problem yields that the columns of W should be constructed from the eigenvectors corresponding to the largest eigenvalues of $S_W^{-1} S_B$. Once transformation is completed, "nearest mean" decision rule is used for classification in the projected subspace.

The first approach to detection and classification problem was to separate the case to different loads. In this experiment, feature vectors obtained from six 2.2 kW motors at three different loading conditions were considered separately resulting three different sets of data. For each load level, the above mentioned classifiers were applied. Classifier performances are evaluated using 40-fold cross validation (shuffled and repeated leave-40-out) so that overall dataset is tested fairly. Classification results for this approach are provided in Tables 1–3, where each classifier result is given in a separate table. The classification results are presented in terms of correct classification percentages followed by the standard deviation (σ) of the classification data.

Although the load conditions may be roughly satisfied for an arbitrary test, fixing the load is not general enough to test the efficiency of the proposed features for arbitrary and practical engineering applications. Hence a second approach is adopted where the data are interpreted regardless of the load and the particular induction motor. Here, notch-filtered data

Table 1
Bayes classification results at motor load of 5, 4.7, and 4.1 A.

	5 A	4.7 A	4.1 A
Healthy	100, $\sigma = 0.00$	99.38, $\sigma = 1.25$	100, $\sigma = 0.00$
rb1	100, $\sigma = 0.00$	100, $\sigma = 0.00$	100, $\sigma = 0.00$
rb2	96.88, $\sigma = 3.75$	93.13, $\sigma = 12.14$	86.25, $\sigma = 7.77$
rot3	100, $\sigma = 0.00$	100, $\sigma = 0.00$	99.38, $\sigma = 1.25$
rot5	98.75, $\sigma = 1.44$	95.63, $\sigma = 4.27$	78.75, $\sigma = 7.77$
sw	100, $\sigma = 0.00$	100, $\sigma = 0.00$	100, $\sigma = 0.00$
Overall	99.27, $\sigma = 0.40$	98.02, $\sigma = 2.19$	94.06, $\sigma = 2.02$

Table 2
GMM classification results at motor load of 5, 4.7, and 4.1 A.

	5 A	4.7 A	4.1 A
Healthy	100, $\sigma = 0.00$	98.75, $\sigma = 1.44$	100, $\sigma = 0.00$
rb1	100, $\sigma = 0.00$	100, $\sigma = 0.00$	100, $\sigma = 0.00$
rb2	98.13, $\sigma = 2.39$	89.38, $\sigma = 15.33$	83.13, $\sigma = 4.27$
rot3	100, $\sigma = 0.00$	100, $\sigma = 0.00$	99.38, $\sigma = 1.25$
rot5	98.75, $\sigma = 1.44$	95.63, $\sigma = 3.15$	75, $\sigma = 12.97$
sw	100, $\sigma = 0.00$	100, $\sigma = 0.00$	100, $\sigma = 0.00$
Overall	99.48, $\sigma = 0.40$	97.29, $\sigma = 2.86$	93.02, $\sigma = 2.81$

Table 3
LDA classification results at motor load of 5, 4.7, and 4.1 A.

	5 A	4.7 A	4.1 A
Healthy	100, $\sigma = 0.00$	98.13, $\sigma = 2.39$	100, $\sigma = 0.00$
rb1	100, $\sigma = 0.00$	100, $\sigma = 0.00$	100, $\sigma = 0.00$
rb2	91.88, $\sigma = 8.26$	60.63, $\sigma = 24.10$	58.13, $\sigma = 8.51$
rot3	100, $\sigma = 0.00$	98.13, $\sigma = 3.75$	100, $\sigma = 0.00$
rot5	91.88, $\sigma = 8.26$	80.00, $\sigma = 14.29$	70.63, $\sigma = 22.02$
sw	100, $\sigma = 0.00$	100, $\sigma = 0.00$	100, $\sigma = 0.00$
Overall	97.29, $\sigma = 0.54$	89.48, $\sigma = 3.31$	88.13, $\sigma = 2.42$

for all three load levels are first normalized by the load current belonging to the respective data. Then the proposed feature vectors were extracted using the normalized data sets. Also, in order to test the ability of developed detection and classification method to work with different motors, in addition to the data of the six 2.2 kW test motors, another 1.1 kW healthy motor data was also normalized by its rated current and added to the total data set. This way, the combined data of two different healthy and five faulty motors data at various loading levels is obtained. It should be noted that a successful identification among this set would correspond to achieving a universal measurement method regardless of the size and load of a particular induction motor. Due to its simplicity and relatively successful behavior, the Bayes classifier is employed to analyze this combined data. Classification results for the combined data with/without 1.1 kW second healthy motor are given in Table 4.

Additionally, statistical significance among three classifiers is computed to quantify and compare the performances of these classifiers. Using average recognition accuracies of classifiers acquired from cross validation tests for all current levels, one-tail paired t-test with a significance level of 0.05 is performed. For this purpose, null and alternative hypothesis are defined as follows:

- Null hypothesis: The mean of average recognition rates for one classifier is the same as rate for the *other* classifier.
- Alternative hypothesis: The mean of average recognition rates for one classifier is greater than the other classifier.

In this way, the probabilities of observing the above mentioned classification results by chance given that the alternative hypothesis is true are obtained as shown in Table 5. The results are given in terms of normalized probabilities. For example, the probability of Bayes classifier being superior than GMM classifier is 66.47%, i.e., Bayes classifier is probably a better method than GMM. If the overall recognition accuracies for all current levels in Tables 1 and 2 are examined, it is verified

Table 4
Bayes classification results using the data normalized around the load current.

	One healthy motor (2.2 kW)	Two healthy motors (2.2 and 1.1 kW)
Healthy	99.58, $\sigma = 1.44$	99.58, $\sigma = 1.44$
rb1	100, $\sigma = 0.00$	97.08, $\sigma = 4.37$
rb2	78.33, $\sigma = 7.77$	70.63, $\sigma = 24.52$
rot3	98.75, $\sigma = 1.44$	97.29, $\sigma = 3.91$
rot5	89.58, $\sigma = 11.52$	89.58, $\sigma = 11.52$
sw	100, $\sigma = 0.00$	96.04, $\sigma = 4.82$
Overall	94.37, $\sigma = 4.82$	91.70, $\sigma = 4.92$

Table 5
Statistical significance among the classifiers.

		Superior		
		Bayes	GMM	LDA
Inferior	Bayes	–	0.3353	0.0011
	GMM	0.6647	–	0.0041
	LDA	0.9989	0.9959	–

Table 6
Confusion matrix for Bayes classification at motor load of (a) 5 (b) 4.7 (c) 4.1 A.

		Predicted					
		hlty	rb1	rb2	rot3	rot5	sw
(a)							
Actual	hlty	160	0	0	0	0	0
	rb1	0	160	0	0	0	0
	rb2	0	0	155	0	5	0
	rot3	0	0	0	160	0	0
	rot5	0	2	0	0	158	0
	sw	0	0	0	0	0	160
(b)							
Actual	hlty	159	0	1	0	0	0
	rb1	0	160	0	0	0	0
	rb2	0	0	149	0	11	0
	rot3	0	0	0	160	0	0
	rot5	0	0	7	0	153	0
	sw	0	0	0	0	0	160
(c)							
Actual	hlty	160	0	0	0	0	0
	rb1	0	160	0	0	0	0
	rb2	0	0	138	0	22	0
	rot3	0	0	0	159	1	0
	rot5	0	0	34	0	126	0
	sw	0	0	0	0	0	160

that Bayes is, indeed, superior to GMM except 5 A current level. Similarly, the probability of LDA classifier being superior than Bayes is just 1.1%, meaning that Bayes classifier is significantly superior to LDA for this purpose. One can verify this situation from Tables 1 and 3 by observing that overall recognition accuracy of LDA classifier is always lower than that of Bayes for all three current levels.

At all motor load levels, confusion matrices for Bayes classification that indicate the distribution of the correct classification, misses, and false alarms are given in Table 6 as a reference.

Most of the work related to motor fault classification depends on spectral features. In order to make a fair comparison and motivate the usefulness of the proposed features, the classification tests are also carried out using spectral features. For this purpose, band-pass energies of the current data are obtained using subband filtering which splits the frequency range

of 0–300 Hz (the significant band that mostly contains discriminative characteristics) into frequency bins of 10 Hz. Mean squared values (the energies) of each bin are selected as the features representing a specific frequency band. Consequently, the feature set contains 30 elements. This dataset is then fed into Bayes classifier to evaluate the performance of spectral features with respect to time-domain features. Classification results including recognition accuracy and standard deviation information are listed in Table 7. The same experiment was repeated using less feature elements (produced frequency bins that are wider than 10 Hz) and cross checked with other classifiers of interest at three load levels. The presented set of results is selected due to its comparable success with the proposed method. Bayes classifier is selected due to the fact that it provides the best recognition results. When these results are compared with the ones obtained with time-domain features, it is apparent that time-domain features offer slightly better accuracy in spite of the significant increase in the dimensionality of feature vectors (30 instead of 4). In fact, if the frequency range is split into only four bins to produce four features, the performance of the spectral method severely deteriorates. It can also be noted that the amount of load seems to have no significant effect on the recognition rate, unlike the case for the proposed parameters. As a conclusion, the

Table 7
Bayes classification results at motor load of 5, 4.7, and 4.1 A using spectral features.

	5 A	4.7 A	4.1 A
Healthy	100, $\sigma = 0.00$	100, $\sigma = 0.00$	100, $\sigma = 0.00$
rb1	98.75, $\sigma = 2.50$	99.38, $\sigma = 1.25$	100, $\sigma = 0.00$
rb2	98.13, $\sigma = 3.75$	99.38, $\sigma = 1.25$	95.63, $\sigma = 3.15$
rot3	98.75, $\sigma = 2.50$	100, $\sigma = 0.00$	98.75, $\sigma = 2.50$
rot5	100, $\sigma = 0.00$	98.75, $\sigma = 1.44$	90.00, $\sigma = 10.61$
sw	83.75, $\sigma = 11.27$	97.50, $\sigma = 2.89$	94.79, $\sigma = 5.10$
Overall	96.56, $\sigma = 2.02$	99.17, $\sigma = 0.59$	94.79, $\sigma = 5.10$

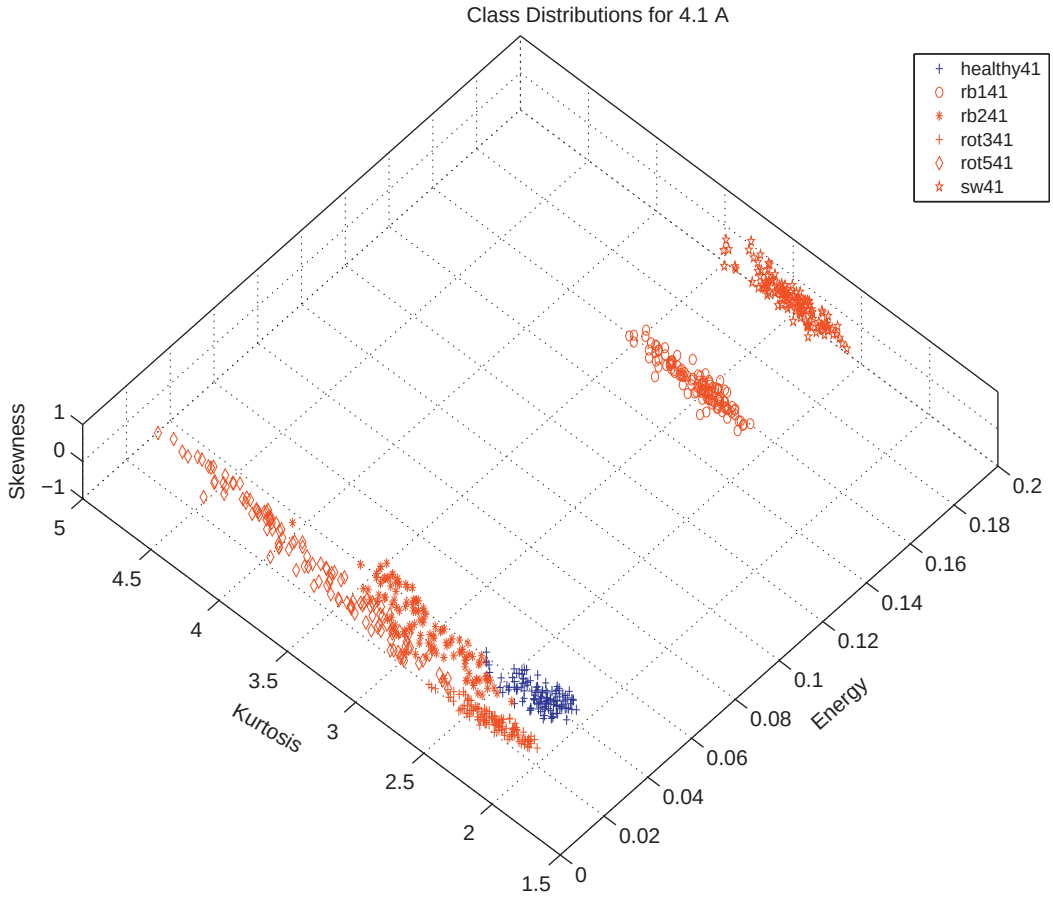

Fig. 6. Feature clusters at 4.1 A.

argument is that the proposed set of time-domain statistical parameters constitute a reasonable feature set with satisfactory classification results.

4.1. Feature analysis under various load conditions

Due to generating the experimental data under laboratory conditions, it was possible to gather current data for various motors with different fault types and different load conditions. Besides, different types of induction motors could also be incorporated into the test set. The deliberate change of load level provided us with interesting observations regarding the feature vector position on the multi-dimensional vector space with respect to the amount of current level for the load. The mentioned behavior could be examined on the three-dimensional space as behavior of the "points" for each constructed feature vector. It is expected that points obtained from the same class motor under the same load should constitute a "cluster" on the three-dimensional feature space, whereas other points from another motor should form a different cluster which could be separated from the previous one using hyper-planes or hyper curves, depending on the type of classifier. The more separated the clusters are for different fault types, the more separable the fault types are. In order to illustrate the situation for the proposed feature set, the mentioned clusters are presented in Figs. 6–8 for load currents of 4.1, 4.7, and 5 A, respectively. The value 4.1 A corresponds to half of the rated load and 5 A corresponds to the full-load.

The analysis regarding the centroid positions of the clusters yields the fact that the centroid loci of the clusters tend to reduce to relatively small energy values as the motor load increases in the case of faulty motors. On the other hand, the healthy motor provides no significant change in any of the features. Although the variance increases (which means that more energy is injected into the faulty parts) as the load decreases, no such change is observed for the healthy motor. For the healthy motor, the energy seems to be equally distributed among all spectral harmonics of the notch-filtered current waveform. For the faulty motors, the distribution somewhat deviates from the Gaussian behavior as the current increases. Interestingly, this deviation unveils itself in different forms for different types of faults. For example, in case of rotor bearing faults, the third order statistical values increase, whereas in case of short circuited stator winding, the fourth order statistics tend to increase more. This provides us with a hint of separating the "type" of fault. The deviation direction of the energy for two example fault cases is indicated by arrows near to the clusters in Figs. 7 and 8.

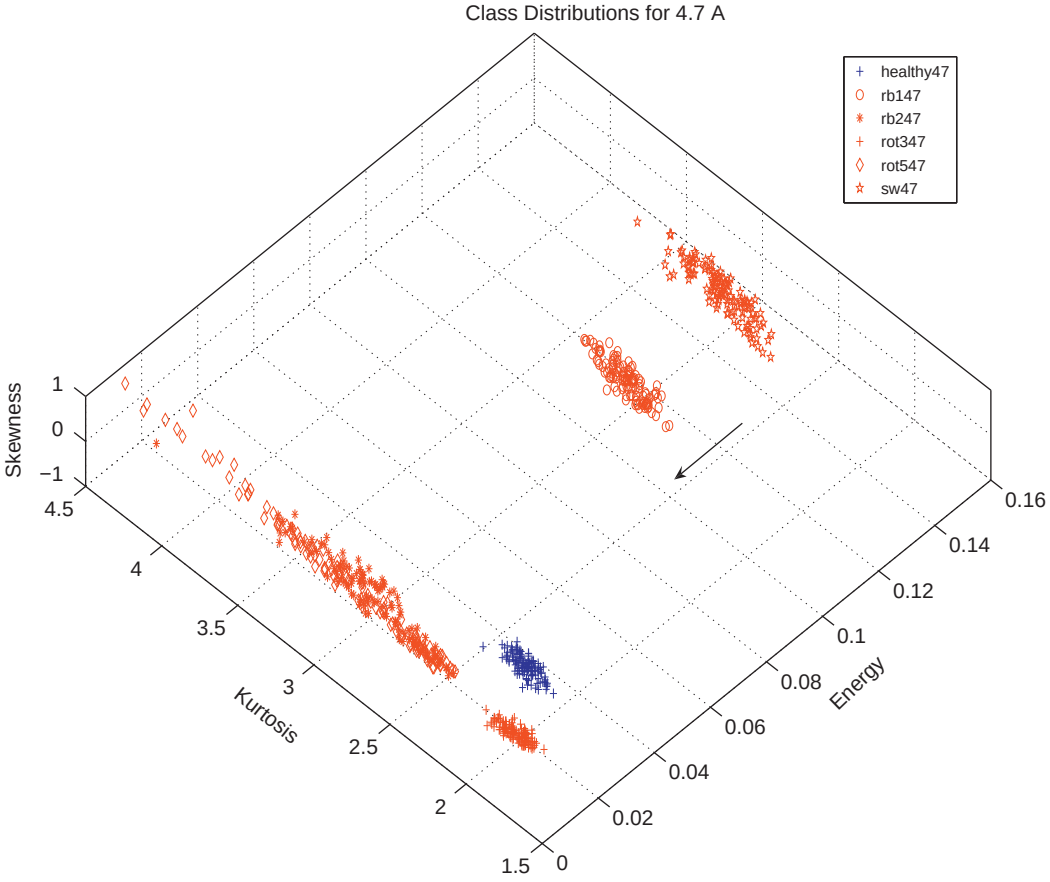

Fig. 7. Feature clusters at 4.7 A.

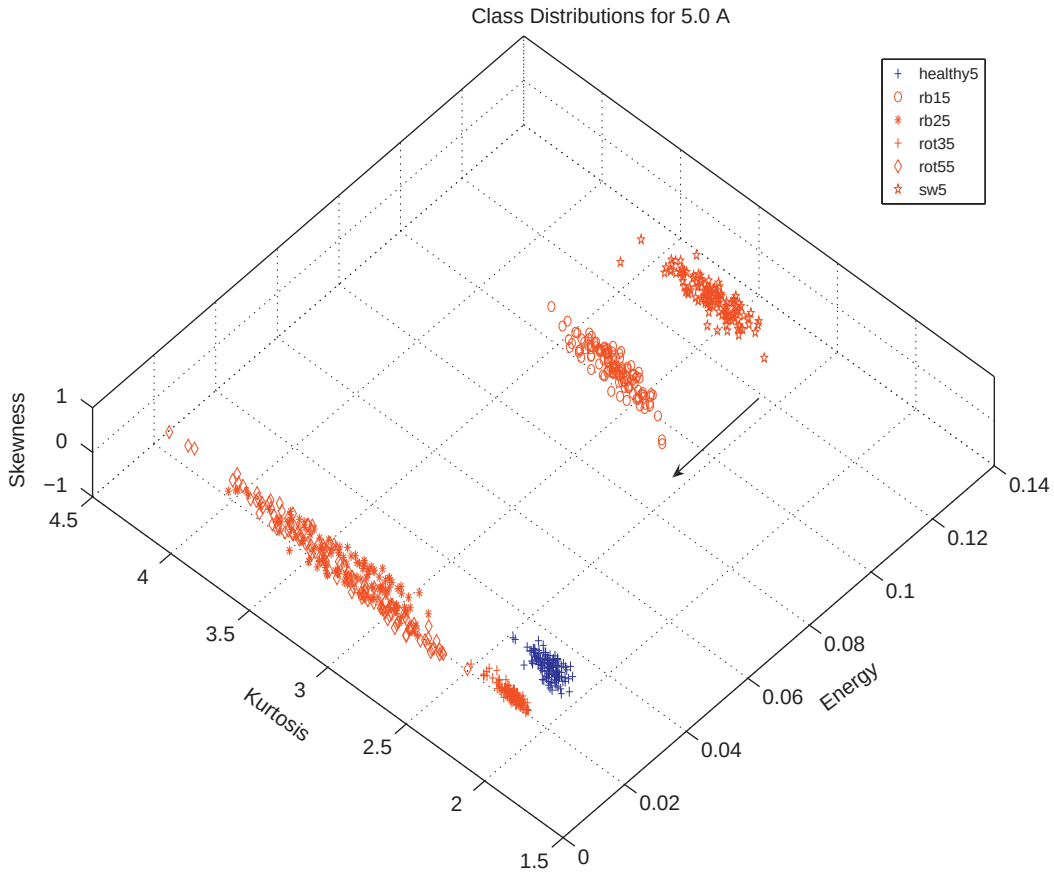

Fig. 8. Feature clusters at 5 A.

The variation of the cluster locations with respect to the cluster of the healthy motor as the load varies is a promising observation regarding the possibility of identifying induction motors with different structures and faults. If a classifier trained for fault detection in one type of induction motor could be suitable for another type of induction motor, then this would be a big step towards achieving a universal measurement system for induction motors. In order to test this capability, a different induction motor (three-phase, 1.1 kW, 380 V, two-pole) is incorporated into the test system. This one is a healthy motor, therefore it is desired to exhibit its feature vectors near or within the cluster limits of the previous healthy motor. Due to the mechanical limitations of the test bed, it was not possible for us to couple the 1.1 kW motor to the generator for loading the motor. Therefore, the parameters for this new healthy motor were acquired under no-load condition. It must be noted that the healthy motors should exhibit similar parametric characteristics regardless of the load condition. Hence, this property is also verified by using a different healthy motor data under no-load condition. In order to compensate for the difference in energy, the current values were normalized by the rated current. Table 4 reveals that the newly added motor is accurately classified within the class of "healthy motors". The three-dimensional plot in Fig. 9 also verifies this result by displaying the cluster of the new healthy motor close to the previous healthy motor. Evidently, the new motor could also be separated from the old healthy motor, however it can still be classified within a unique convex cell together with the previous healthy motor. Despite the significant differences in the load level and the name plates, two different healthy motors still cluster together in the same feature space which enables them to be distinguished from other faulty motors considered here. This observation may indicate that the proposed method is a versatile approach for induction motor condition monitoring.

Despite the lack of faulty motors from the type of the second motor, it can be estimated that such faulty motors would not necessarily provide feature clusters near to the features of other motors with the same fault class. Faults are stochastic processes that may exhibit their features at different levels. Therefore, it is difficult to claim exact classification of the fault type regardless of the type of induction motor, and regardless of the exact physical location or type of the fault. On the other hand, it is evident that "any" fault perturbs the notched current waveform from Gaussianity in terms of increased third and fourth order statistics. Clearly, the leakage of the injected energy into harmonic components other than the fundamental increases with the existence of a motor fault. However, when the load increases, the amount of injected

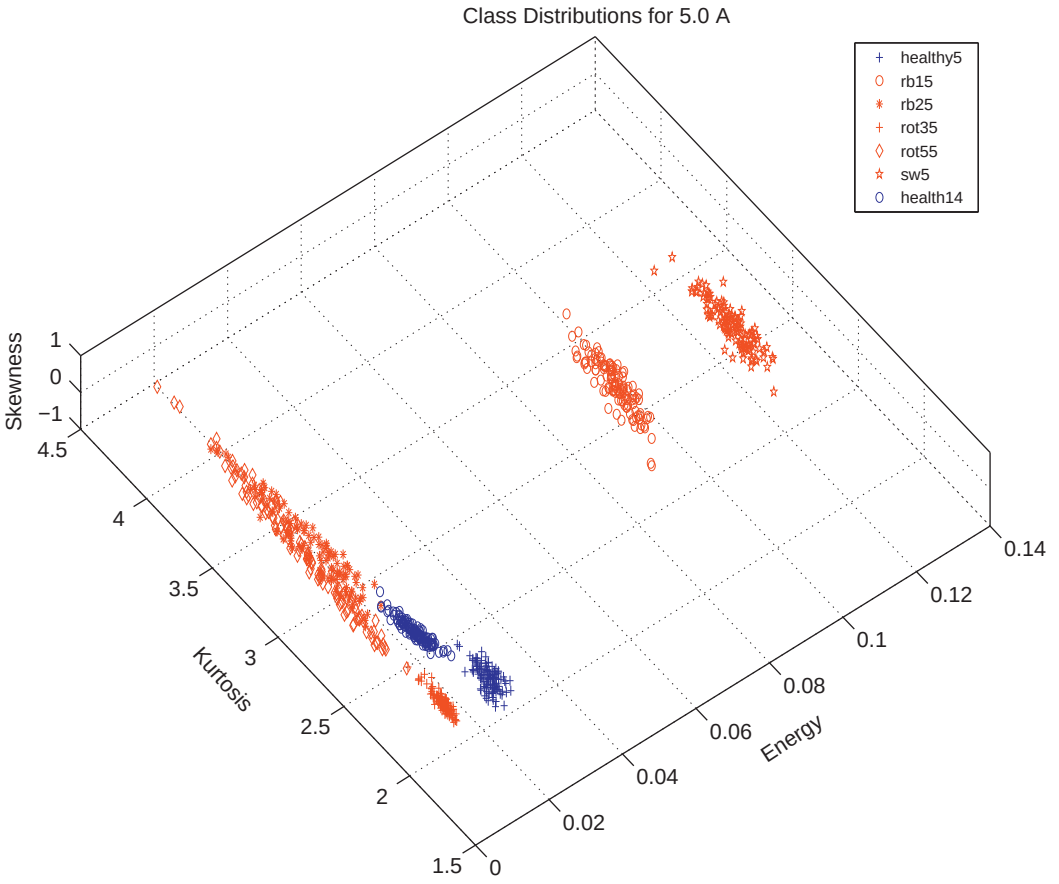

Fig. 9. Feature clusters of motors including the new healthy motor.

energy into the non-fundamental harmonics also increases. In order to distinguish between the two cases, the statistical distribution of the notched current waveform is analyzed and successful indicators were obtained.

5. Conclusions

In this study, notch-filtered motor current signature analysis is proposed and applied for the analysis of induction motor condition monitoring. The distinguishing approach in this article is to utilize only localized time-domain information instead of employment of spectral information (such as Fourier or wavelet domain) which are commonly used in most of the previous works. The time-domain features used herein are namely the energy, sample extrema, and skewness and kurtosis evaluated from data within sliding time window. Exhaustive testing is performed in order to observe the classification accuracy of the proposed features using six identical three-phase induction motors and an additional structurally different motor. Experimental verification of the proposed features and classifiers reveal that NFMCSA approach is a promising analysis especially considering the fact that high classification accuracy can be achieved even in case of structurally different machines with numerous different faults under varying motor load conditions.

The mathematical modeling of the analytical behavior of features with respect to changing load conditions, various motor types, and numerous fault classes using the proposed feature set remains to be an interesting future work.

References

[1] G.G. Acosta, C.J. Verucchi, E.R. Gelso, A current monitoring system for diagnosing electrical failures in induction motors, Mechanical Systems and Signal Processing 20 (2006) 953–965.
[2] S. Nandi, H.A. Toliyat, X. Li, Condition monitoring and fault diagnosis of electrical motors—a review, IEEE Transactions on Energy Conversion 20 (4) (2005) 719–729.
[3] A. Siddique, G.S. Yadava, B. Singh, A review of stator fault monitoring techniques of induction motor, IEEE Transactions on Energy Conversion 20 (1) (2005) 106–114.
[4] B. Ayhan, M.Y. Chow, M.H. Song, Multiple signal processing-based fault detection schemes for broken rotor bar in induction motors, IEEE Transactions on Energy Conversion 20 (2) (2005) 336–343.

[5] Z. Zhang, Z. Ren, W. Huang, A novel detection method of broken rotor bars based on wavelet ridge, IEEE Transactions on Energy Conversion 18 (3) (2003) 417–423.
[6] H. Douglas, P. Pillay, A.K. Ziarani, Broken rotor bar detection in induction machines with transient operating speeds, IEEE Transactions on Energy Conversion 20 (1) (2005) 135–141.
[7] A.M. Knight, S.P. Bertani, Mechanical fault detection in a medium-sized induction motor using stator current monitoring, IEEE Transactions on Energy Conversion 20 (4) (2005) 753–760.
[8] M.H. Benbouzid, G.B. Kliman, What stator current processing-based technique to use for induction motor rotor fault diagnosis, IEEE Transactions on Energy Conversion 18 (2) (2003) 238–244.
[9] D.-M. Yang, A.F. Stronach, P. MacConnell, J. Penman, Third-order spectral techniques for the diagnosis of motor bearing condition using artificial neural networks, Mechanical Systems and Signal Processing 16 (2–3) (2002) 391–411.
[10] N. Arthur, J. Penman, Induction machine condition monitoring with higher order spectra, IEEE Transactions on Industrial Electronics 47 (5) (2000) 1031–1041.
[11] R. Yan, R.X. Gao, Hilbert–Huang transform-based vibration signal analysis for machine health monitoring, IEEE Transactions on Instrumentation and Measurement 55 (6) (2006) 2320–2329.
[12] H. Douglas, P. Pillay, A.K. Ziarani, A new algorithm for transient motor current signature analysis using wavelets, IEEE Transactions on Industry Applications 40 (5) (2004) 1361–1368.
[13] R.R. Schoen, T.G. Habetler, Effects of time-varying loads on rotor fault detection in induction machines, IEEE Transactions on Industry Applications 31 (4) (1995) 900–906.
[14] R.O. Duda, P.E. Hart, D.G. Stork, Pattern Classification, Wiley, USA, 2001.
[15] A.C. McCormick, A.K. Nandi, Bispectral and trispectral features for machine condition diagnosis, IEE Proceedings—Vision Image and Signal Processing 146 (5) (1999) 229–234.
[16] A.C. McCormick, A.K. Nandi, Cyclostationarity in rotating machine vibrations, Mechanical Systems and Signal Processing 12 (2) (1998) 225–242.
[17] R.A. Fisher, The use of multiple measurements in taxonomic problems, Annals of Eugenics 7 (1936) 179–188.